Total Experimental Uncertainty in Hydrodynamic Testing of a Semisubmersible Wind Turbine, Considering Numerical Propagation of Systematic Uncertainty

Amy Robertson*[a], Erin E. Bachynski[b], Sebastien Gueydon[c], Fabian Wendt[a], Paul Schünemann[d]
*Corresponding Author, email: Amy.Robertson@nrel.gov

[a]National Renewable Energy Laboratory, 15013 Denver West Parkway, Golden, CO 80401
[b]Norwegian University of Science and Technology (NTNU) Department of Marine Technology, Marine Technology Center, 7491 Trondheim, Norway
[c]MARIN, 2, Haagsteeg, P.O. Box 28, 6700AA Wageningen, The Netherlands
[d] Universität Rostock, Lehrstuhl für Windenergietechnik, Fakultät für Maschinenbau und Schiffstechnik, Albert-Einstein-Straße 2, 18059 Rostock, Germany

Abstract

Quantifying the uncertainty in experimental results is a critical step in properly validating numerical simulation tools for designing floating wind turbines; without a good understanding of the experimental uncertainties, it is impossible to determine if numerical simulation tools can capture the physics with acceptable accuracy. Recent validation studies suggest that the wave-induced, low-frequency surge and pitch motions of semisubmersible-type floating wind turbines are consistently underpredicted by numerical simulations, but it has not been possible to state whether or not this underprediction is within the level of experimental error. In the present work, previously assessed systematic uncertainty components in hydrodynamic tests of the OC5-DeepCwind semisubmersible are propagated to response metrics of interest using numerical simulation tools, and combined with the random uncertainty to obtain the total experimental uncertainty. The uncertainty in the low-frequency response metrics is found to be most sensitive to the system properties (e.g., mooring stiffness and center of gravity), but also the wave elevation. The results of the present study suggest that the underprediction of the low-frequency response behavior observed in previous validation studies is larger than the experimental uncertainty.

Keywords: Floating Offshore Wind, Uncertainty Analysis, OC5, Validation, Nonlinear Wave Mechanics

1 Introduction

Floating wind turbines (FWTs) represent a growing area of both academic and industrial interest, and a wide range of numerical tools have been developed to predict their responses in wind and waves. Recently, participants in the international Offshore Code Comparison Collaboration, Continued, with Correlation (OC5) project attempted to validate models of a floating semisubmersible tested in the offshore basin at MARIN (in May 2013) by the DeepCwind consortium (Goupee et al. 2014). Although state-of-the-art tools captured some of the dynamics and loads of the complex floating wind turbine, there were persistent differences between the simulated results and measurements, the reasons for which could not be ascertained.

The discrepancies are exemplified by an under-prediction of the ultimate and fatigue loads across multiple load cases, which were shown to be dominated by the under-prediction of the loads at the pitch and tower natural frequencies (Robertson et al. 2017). Similar discrepancies in the low-frequency response of other model-scale semisubmersible platforms for offshore wind have also been observed (Cermelli and Roddier 2005, Philippe et al. 2013, Berthelsen et al. 2016). In order to assess whether or not the observed differences between numerical and experimental results are meaningful, an assessment of the level of experimental uncertainty in the response behavior needs to be determined.

To that end, additional testing of the semisubmersible structure from the OC5 study (in a simplified configuration) was carried out at MARIN through the MaRINET2 grant. These simplified tests were aimed toward better understanding the hydrodynamic loading and assessing uncertainty in the test campaign. The generic open-access design (OC5-DeepCwind floating semisubmersible) was tested at 1/50 scale with the same floating substructure as was examined in OC5, but with a rigid tower, a mass representing the rotor-nacelle assembly, and with a simplified soft-spring mooring system representing the linear stiffness of the original catenary configuration. The wind turbine and flexible tower were replaced by rigid components to limit uncertainty sources and better focus on the hydrodynamic loading on the structure. Due to the limited testing time in the basin, a single configuration was considered, and a limited number of wave conditions were tested (Gueydon 2017). Extensive repetition tests were included in the test matrix to assess the random uncertainty in the experiment.

Response metrics, low-dimensional representations of the important features of the time series of results, are used to represent the results and the associated uncertainty. The experimental uncertainty originates from uncertainties in the excitation of the system and the properties of the test specimen, and the

accuracy and precision of the measurement equipment. Several standards provide guidance on uncertainty assessment, such as the International Standards Organization (ISO, 1993), American Society of Mechanical Engineers (ASME, 2013), and The International Towing Tank Conference (ITTC, 2008). Here, we apply the ASME terminology, categorizing the sources of uncertainty as either random or systematic. Systematic uncertainties may result in an unknown bias in the test, while random uncertainties result in randomly varying uncertainties which can be measured through repetition tests.

The contributions to the experimental uncertainty in the new set of tests were identified and documented in previous work (Robertson et al. 2018). Among the main findings, it was shown that the uncertainty in the wave elevation was small, and was dominated by the random uncertainty. It should be noted, however, that the uncertainties in the wave loads (not measured) may be larger than the uncertainties in the wave elevation. The physical properties of the model itself were found to have more significant systematic uncertainties, and the measurement cable contributed significantly to the uncertainty in the mass and in the center of mass. The measurement of motion responses was precise, while the tension measurements had relatively high random uncertainty.

The present work seeks to identify the total uncertainty of the response metrics of interest. This is accomplished by first propagating the systematic uncertainties to the response metrics through numerical simulations, and then combining with the calculated random uncertainty. Three state-of-the-art simulation tools – applied by four different users, and considering several modeling approaches – were used to assess the consequences of changes in the input parameters (corresponding to the systematic uncertainty levels) on responses such as the low-frequency surge and pitch motions and wave-frequency surge and pitch motions. In the remainder of the paper, the model tests and response metrics of interest are briefly described (Sections 2 and 3). Next, the uncertainty sources identified by Robertson et al. (2018) are summarized, and the most important of these are identified (Section 4). The methodology for propagating systematic uncertainties is explained, and the total uncertainty is examined (Sections 5 and 6).

2 Test Description

The floating semisubmersible model consisted of the existing MARIN model 9697, whose geometry corresponds to the DeepCWind semisubmersible floater (Goupee et al. 2012) at 1/50 scale, and a rigid aluminum tower designed to mimic the mass and inertia of the NREL 5 MW wind turbine tower and rotor-nacelle-assembly (Jonkman et al. 2009, Jonkman 2010). A brief overview of the model setup (Figure 1) is given here; additional details may be found in Robertson et al. 2018. The test setup and all results are presented at full scale, following Froude scaling. The difference in density between sea water (1025 kg/m^3) and fresh water in the basin (998.6 kg/m^3) is accounted for in the scaling of masses, inertias, forces, moments, and derived quantities.

A simplified mooring system was designed and constructed for the new tests. Three mooring lines, consisting of a soft spring and rigid wire, were attached to the model. A pulley system was used such that the spring could be vertical and dry, while the anchor positions were low enough that the surge-pitch coupling from the mooring system was similar to the original catenary system.

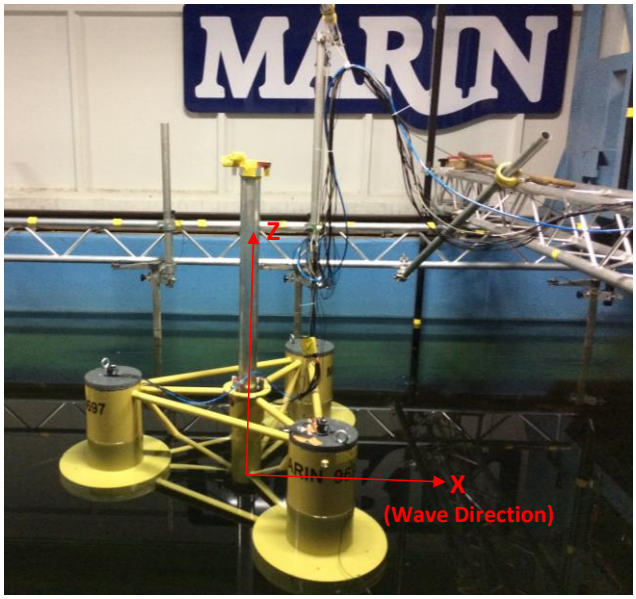

Figure 1: Floating test set-up. Waves propagate from left to right in this figure, and positive surge motion is defined in the same direction as the wave propagation (Image by: Amy Robertson).

2.1 Model Properties

The main characteristics of the floater geometry are shown in Table 1, while the hydrodynamic properties and mass properties are given in Table 2 and Table 3, respectively. The mooring system, which included thin wires attached to springs, is described in Table 4.

Table 1: Key geometric parameters

GEOMETRIC PROPERTIES	
Center column diameter [m]	6.5
Side column diameter [m]	12.0
Base column diameter [m]	24.0
Draft [m]	20.0
Base column height [m]	6.0
Side column freeboard [m]	10.0
Tower top height over keel [m]	77.3

Table 2: Hydrodynamic properties

HYDRODYNAMIC PROPERTIES	
Water depth [m]	180.0
Water density [kg/m^3]	1025.0
Displaced volume [m^3]	14040

Table 3: Masses and inertia of entire system (tower+platform). CG: center of gravity.

MASSES/INERTIAS	
Overall system mass [kg]	1.4196E+7
Overall system CG (z) [m below SWL]	7.53
Ixx abt system CG [kg-m^2]	1.2898E+10
Iyy abt system CG [kg-m^2]	1.2851E+10
Izz abt system CG [kg-m^2]	1.4189E+10

Table 4: Mooring line properties. EA: Young's modulus multiplied by cross-sectional area.

MOORING LINES	
Line angle [deg]	55.5
EA [N]	2.7106E+6
Unstretched line length [m]	55.432
Preload [kN]	1122.5

Mooring stiffness [kN/m]	48.9

When modelling the system numerically, we strived to use the properties of the system as measured, where possible. For a floating system, the first step is to ensure that the system is in equilibrium for the prescribed values of the draft, mass, mooring tensions, and displaced water volume. For this test, we directly measured the draft, mass, and tensions. The displaced water volume can be calculated from the geometry, but since it is not directly measured, we considered this property as the most unknown. We did not tune the other properties mentioned, but prescribed the displaced water volume such that the system was in equilibrium (Table 5).

Table 5: Balance of Vertical Forces

BALANCE OF VERTICAL FORCES	
Total vertical mooring force [N]	-1.9074E+06
Total gravity force [N]	-1.3922E+08
Displacement needed for equilibrium [m^3]	**14040**
Buoyancy Force [N]	1.4113E+08
SUM [N]	0.0000E+00

2.2 Test Matrix

The tests in this campaign included a hammer test, free decay tests and wave excitation tests. Only the wave excitation tests are of interest here, and are summarized in Table 6. As shown, multiple repetitions were carried out for the model in waves, which will be used to assess the random uncertainty in the response behavior. The repetitions were performed with the same wave realization, with the goal of~~have~~ having ~~the~~ identical wave time series.

Table 6: Te~~s~~t matrix – wave cases.

Test Name	**Waves**	**Number of repetitions**
Regular wave 1	H=7.1 m, T=12.1 s	5
Regular wave 2	H=4 m, T=9 s	2
White noise	Hs=7.1 m, T=6-26 s	2
Irregular wave	Hs=7.1 m, Tp=12.1 s	5

Formatted Table

3 Response Metrics

The objective of the larger validation campaign related to these experiments is to better understand the ability of simulation tools to predict the response of the OC5-DeepCwind semisubmersible to hydrodynamic loading, especially the low-frequency (resonant) responses in pitch and surge. To assess the capabilities of the tools in this area, response metrics were identified to represent these important physical quantities of interest. The response metrics are scalar values that can be computed from the time series results from either simulations or experiments. A simulation tool that can reproduce the response metrics within the obtained uncertainty bounds can then be considered validated.

The response metrics in the present work focus on the surge, heave, and pitch responses of the semisubmersible, in particular: the mean response in surge, and the wave-frequency and low-frequency responses in all three degrees of freedom. The response metrics are chosen with the objective of representing these different response components, rather than selecting metrics that are useful for design (such as the 90th percentile maximum 3-hour motions), but do not distinguish among different frequency ranges.

The response metrics in the present work are:

M1. **RAO**: the response amplitude operator (RAO) in surge, heave, and pitch at 6 discrete frequency points within the wave energy range;
M2. **PSD Sum, Low Frequencies**: the integral of the power spectral density (PSD) of surge and pitch motions over the low-frequency range;
M3. **PSD Sum, Wave Frequencies**: the integral of the PSD of surge and pitch motions over the wave-frequency range and
M4. **Mean Surge Offset**.

For all of the metrics, only a limited time window of the analysis is considered (Table 7), in an attempt to focus on data after start-up transient behavior and also address the effect of reflected waves. The irregular wave window consists of the last three hours (after reflections are established), while the regular wave window includes 10 minutes of data once the ramp in the waves has passed but before any reflections arrive from the beach or wavemaker. Furthermore, all of the time series are resampled with a time step of 0.1 s prior to computing any metrics. Response metrics M2 and M3 are only computed for the irregular wave cases.

Table 7: Time windows for calculation of response metrics

Wave	Start of window	Duration of window
Regular wave 1	600 s	600 s
Regular wave 2	1000 s	600 s
White noise	1870 s	10800 s
Irregular wave	1870 s	10800 s

Metric M1, the RAO, is defined as the amplitude of the response divided by the amplitude of the incoming wave at a given frequency. Six discrete frequencies are considered for the RAO calculations, as shown in Table 8.

Table 8: Wave frequencies for RAO calculations

Frequency Pt.	Frequency	
1	0.065 Hz	
2	0.075 Hz	
3	0.0826 Hz	Frequency of regular wave 1
4	0.095 Hz	
5	0.105 Hz	
6	0.1105 Hz	Frequency of regular wave 2

The algorithm applied for computing the RAO, denoted $H(\omega)$, is based on the cross spectral density:

$$H = \frac{yu^*}{uu^*}$$

where u and y are the Fourier transforms of the wave elevation and the motion response, respectively, and the asterisk indicates the complex conjugate.

The integrals of the PSDs of the response (referred to as "PSD sums" – metrics M2 and M3) are chosen to capture frequency-dependent responses both in and outside the wave frequency range in irregular sea states. Compared to other possible metrics, such as RMS values, this approach keeps some frequency information. When calculating the PSD sums, all time series (measured and simulated) are first cut and sampled such that they have identical discretization in time (time step and duration). The same PSD

calculation algorithm, without smoothing, is then applied to all time series. The PSD sums are computed based on the one-sided, unsmoothed, discrete power density functions:

$$S_{sum} = \sum_{i=j}^{k} S_{resp}(f_i)\,\Delta f$$

where S_{resp} is the discrete power spectral density of the response at frequency f_i, Δf is the corresponding frequency increment, j is the index of the first frequency of interest, and k is the index of the last frequency of interest. The frequency limits for the low- (M2) and wave-frequency (M3) components of the spectrum are given in Table 9. These are based on identifying the ranges over which the wave spectra were defined, and then encompassing the lower frequencies below that range, without considering the zero-frequency mean value.

Table 9: Frequency limits for summation of power spectral density function for response metrics M2 and M3

Wave	Low-frequency window	Wave-frequency window
White noise	0.005 Hz – 0.038 Hz	0.038 Hz – 0.14 Hz
Irregular wave	0.005 Hz – 0.05 Hz	0.05 Hz – 0.14 Hz

4 Uncertainty Sources

4.1 Random Uncertainty

Robertson, et al. (2018) identified a number of sources for random uncertainty in the response metrics. However, since repeated measurements of the quantities of interest were available, the random uncertainty could be calculated directly from the measurements without the need to assess the source of the uncertainties. The random standard uncertainty, $s_{\bar{x}}$, is calculated as the standard deviation, s_x, of the metric (X) across the repeated tests, divided by the square root of the number of observations (N):

$$s_{\bar{x}} = \frac{s_x}{\sqrt{N}}$$

4.2 Systematic Uncertainty

Systematic uncertainty is a representation of the possible bias in a test campaign, and cannot be calculated directly from measurements. Instead, the sources of systematic uncertainty throughout the test must be identified, their individual effect on the metrics calculated, and then those effects combined. The sources of uncertainty in this test campaign include the wave excitation, system properties and configuration, and output measurements. Expert analysis of the systematic uncertainties in the test campaign identified 24 separate parameters with significant levels of systematic uncertainty. These parameters are listed in Table 10. Robertson, et al. (2018) provide a thorough discussion on the assessment of the uncertainty levels for these parameters.

Table 10: Sources of systematic uncertainty. CM: center of mass.

	Parameter	Baseline Value	Uncertainty Level
1	Platform mass [kg]	1.4196E+7	8.75E+4
2	CM, x direction [m]	0	0.22
3	CM, y direction [m]	0	0.22
4	CM, vertical [m]	-7.53	0.21
5	Platform inertia, Ixx abt CM [kg-m^2]	1.2898E+10	1.2898E+8
6	Platform inertia, Iyy abt CM [kg-m^2]	1.2851E+10	1.2851E+8
7	Platform inertia, Izz abt CM [kg-m^2]	1.4189E+10	1.4189E+8
8	Draft [m]	20	0.25
9	Column angle, [deg]	0	0.5
10	Column diameter, [m]	12 or 24	0.1
11	Mooring stiffness [kN/m]	48.9	5.2
12	Mooring pretension [kN]	1122.5	62
13	Anchor position x [m]	Radially outward	0.25

14	Anchor position y [m]	Radially outward	0.25
15	Anchor position z [m]	Up/down	0.25
16	Mooring fairlead position [m]	Radially outward	0.05
17	Initial position [m]	0	0.12
18	Initial orientation [deg]	0	0.062
19	Water depth [m]	180	2
20	Water density [kg/m^3]	1025	10.25
21	Wave elevation – due to sensor drift [m]	measured	0.03
22	Wave elevation – due to probe location and tilt [m]	measured	negligible
23	Translation measurement [m]	0	0.03
24	Rotation measurement [deg]	0	0.3

From this original set of systematic uncertainty sources, the parameters were down-selected based on their influence on the response metrics. They were thresholded by examining the total combined estimated systematic uncertainty of the response metrics. Parameters whose effect on the change across all metrics was less than 10% were removed. In the end, the original set of 24 parameters was down-selected to 8, which are summarized in Table 11. Note that only parameters related to the system properties and configuration remain in the list, and no measurement or wave excitation uncertainties are included.

Table 11: Selected parameters for uncertainty propagation

	Parameter	Abbreviation
1	Center of mass, x direction	CMx
2	Center of mass, vertical	CMz
3	Mooring stiffness	Stiff
4	Draft	Draft
5	Column diameter	ColDia
6	Wave elevation – due to sensor drift	WaveElev
7	Platform inertia, Iyy abt CM	Iyy
8	Platform mass + Displaced Volume	Mass+Buoy

In this new list, when the platform mass was changed, the displaced volume was adjusted to ensure the heave equilibrium position was not altered. The goal was to have each of these parameters be independent of one another. If just the mass were altered, the draft would have changed, which is a separate parameter.

Many of these variations act on the response of the system without directly changing the wave excitation. Variation 1 increases the cross-coupling of inertia contributions (surge/pitch, heave/pitch). Variations 2 and 7 change the inertia moment in pitch and consequently the pitch natural period. Variation 3 results in a change of the surge natural period. On the other hand, variations 4, and 5 directly affect the wave excitation by changing the volume exposed to the waves, while also changing the pitch natural period. For variation 4, the pitch period is modified through the shift of the buoyancy point and the variation of displacement. Variation 5 results in a change in the metacentric height and hence in the pitch period. Variation 8 affects the surge and heave natural periods, while variation 6 only affects the wave excitation.

5 Uncertainty Propagation

"Uncertainty propagation" is determining the sensitivity of the output response to the input and model uncertainties. If a closed-form solution is known for this relationship, then the uncertainty can be propagated analytically. However, for complex problems such as the dynamics of a floating offshore wind system, a closed-form solution may not be available. In these situations, numerical methods can be used instead. A common approach is to use a Monte Carlo approach to sample the input uncertainty distribution, and calculate the effective output distribution. The calculation itself can be accomplished through simulation of a numerical model of the system. Reduced-order models are of often used because of their computational efficiency, e.g., polynomial chaos expansion (Murcia, et al. 2017) and machine learning techniques (Clifton, et al. 2014). An even simpler method is sequential perturbation (Manteufel, 2012 and Figliola and Beasley, 2011), which requires just two simulations at the bounds of the input or model uncertainty to assess the uncertainty bounds on the response metric of interest. Sequential perturbation is used here to limit the computation time and maintain the use of sufficiently accurate models. ~~Carlo analysis with a reduced-order model was not considered as the authors believed that this would~~

The process of using a model to propagate uncertainty can be problematic because it relies on the use of the modeling tools that are to be validated to perform the uncertainty propagation. If the tools do not represent the phenomena of interest accurately, they may not provide an accurate assessment of the sensitivity of parameter variations on that phenomena. To address this issue, multiple numerical modeling tools and multiple modeling approaches were used to propagate the uncertainties in this work. The largest positive and negative contributions (out of all simulation approaches) are then used as the sensitivity coefficient for each parameter of interest. Within the limits of the numerical models, this approach is expected to give a conservative estimate of the uncertainty for validation purposes. ~~systematic uncertainty sources in Table 11 are independent of each other.~~

5.1 Approach

The systematic uncertainty of an output response metric, b_R, is calculated by combining each of the elemental systematic output standard uncertainties, b_i.

$$b_R^2 = \sum_{i=1}^{N} b_i^2$$

For the systematic uncertainties related to the input waves or model properties, these uncertainty values (d_i) must be first propagated to their effect on the response metric uncertainty:

$$b_i = \theta_i \, d_i$$

where $\theta_i = \partial X / \partial p_i$ are the sensitivity coefficients of individual parameters, p_i, on the metric of interest, X; and, d_i are the elemental input/model systematic uncertainties (as summarized in Table 11). Once propagated, each of the output metric uncertainty sources may be summed. The sensitivity coefficients represent the influence that the input/model uncertainties have on the output metrics, and are typically calculated analytically; but, if that is not possible, numerical models of the system can be used to estimate them.

In this work, the systematic uncertainty of the response metrics due to a given uncertainty source is estimated by sequential perturbation by first simulating the model using the baseline properties and calculating the associated response metrics. Then, the system is simulated using a new value for one of the six uncertain parameters, based on the uncertainty level described in Table 11 (changes are made in both the positive and negative directions), and the response metrics are again calculated. The difference between the response metrics calculated using the baseline properties and when changing one of the uncertain parameters is the systematic uncertainty for that parameter. Systematic uncertainties will be calculated based on both a positive and negative change in the parameter, and the resulting level of propagated uncertainty may not be the same (see Section 5.2). This process is repeated for all six parameters, and then those individual uncertainty sources combined in quadrature. This method assumes that each of the systematic uncertainty sources in Table 11 are independent of each other.

~~This process can be problematic in that it relies on the use of the modeling tools that are to be validated~~

Asymmetric Uncertainty

The propagation results in non-symmetric uncertainty bounds for the metrics; meaning that the uncertainty on the positive end is sometimes different from the level on the negative end of the metric value. This situation creates a complication in combining the different systematic uncertainty sources as the straightforward method of adding them in quadrature no longer works. Different approaches can be

Commented [AR1]: Move up front.

Field Code Changed

used to address this. The simplest approach is to add the negative uncertainty bounds in quadrature, and the positive uncertainty bounds in quadrature, separately; but, this approach has been shown to be inaccurate. Another approach is proposed by Dieck (2007) and uses the calculation of a central value for the nonsymmetric uncertainty bounds, which is then used to adjust the final uncertainty summed across multiple sources. This approach was used here. The systematic response metric uncertainty, b_i, for an individual parameter (i) is calculated as:

$$b_i = \frac{(\bar{X} + b_i^+) - (\bar{X} - b_i^-)}{2}$$

where $\bar{X}$ is the mean measured value for a given metric. The total estimated systematic standard uncertainty, b_R, is then calculated. The asymmetry of the systematic uncertainty is further addressed in the calculation of the total uncertainty (Section 6.1).

5.45.3 Modeling Tools / Methods

Three different simulation tools were used to propagate the systematic uncertainty in the model properties to the response metrics, and several different users contributed results. A variety of tools and users was employed since the approach used to model the behavior of the floating wind system may affect the propagation of uncertainty. Ideally, the modeling tools that are to be validated would not be the same ones used to perform the uncertainty propagation, but this is the only option for a complex system such as a floating wind turbine. The largest propagated uncertainty found across the different tools and users was used to help assuage this limitation.

All of the simulation approaches represent the floating wind system as a rigid body with linear elastic mooring lines. For the hydrodynamic loading, second-order diffraction is considered in addition to first-order potential flow contributions (added mass, radiation damping, and excitation). The smaller braces and pontoons were ignored in the potential flow solution. Different meshes and potential flow solvers were used (WAMIT – WAMIT, 2011 and DIFFRAC – Buchner, 2001), and so the first- and second-order potential flow solutions differ among the simulation approaches. Overall, when the same modeling approach is used (but different modeling tools), there is reasonable agreement of the wave and low-frequency motions (Gueydon et al, 2014); however, differences in the modeling of the first-order and second-order wave excitations and damping lead to differences in the motion responses, especially around the resonance frequencies in surge, heave and roll/pitch (Robertson et al, 2017).

For this study, five modeling approaches were followed with three distinct simulation tools to propagate deviations in the set of parameters of Table 11. The main differences between these modeling approaches are summarized in Table 12. Two fundamentally different approaches were used to account for linear and quadratic damping effects. A subset of the numerical models used Morison-type drag to compute quadratic damping loads on the substructure members (FAST, SIMA, aNySIM), while another subset of models used a tuned linear (P) and quadratic damping (Q) matrix (FAST_PQ, aNySIM_PQ), also referred to as the PQ-approach in this paper. The tuning was conducted based on decay tests in surge, heave and pitch. The PQ-approach was included here because it has demonstrated improved model predictions for the low-frequency pitch motion response of the system in past projects (Gueydon, 2016). The corresponding damping matrices are shown in Table 13.

Table 12: Numerical modelling approaches

Model ID	Global linear and quadratic drag	Morison drag on vertical columns	Morison drag on heave plates	Wave loads above still water level
FAST		x	x	Morison-type drag up to 1st order free surface based on constant potential
FAST_PQ	x			
SIMA		x	x	Morison-type drag up to 1st order free surface based on constant potential
aNySIM			x	Morison loads applied on heave plate only, Therefore, no wave loads act above still water level.
aNySIM_PQ	x			

Table 13: Global linear and quadratic damping coefficients applied in the PQ modelling approaches.

DOF	Linear Damping	Quadratic Damping
Surge	1.83E+5 N/(m/s)	0.0 $N/(m/s)^2$
Heave	0.0 N/(m/s)	3.04E+6 $N/(m/s)^2$
Pitch	6.47E+7 Nm/(rad/s)	2.26E+10 $Nm/(rad/s)^2$

Furthermore, the models using Morison elements don't apply the coefficients identically: the location of these elements and values of the coefficients are different. While all five models accounted for second-order difference frequency diffraction, the quadratic transfer functions (QTF) are different. The quadratic terms of the QTF used in the aNySIM and aNySIM_PQ simulations were updated based on the motion RAO of the floater of the present study, while all other simulations were performed with QTFs based on the OC5-DeepCwind system (Robertson et al. 2017). Even though none of these models is perfect, it is assumed that the choice of several tools and modeling approaches should enable an assessment of realistic trends for the propagation of the uncertainty linked to the 8 most influential parameters of Table 11.

Figure 2- Figure 5 show a comparison of the PSDs of the surge and pitch responses for the experimental measurements and the baseline simulations. The integration limits for the low-frequency and wave-frequency PSD sums are illustrated using the colored pink and blue regions in the plots. As shown, the responses around the natural frequencies in surge (~0.01 Hz) and pitch (~0.03 Hz) are significant compared to the wave-frequency responses, and the experimental measurements show high levels of repeatability in the experiments. Figure 6 compares the PSD sum metrics (calculated from these values) between experiment and baseline simulations.

The wave-frequency surge and pitch responses are captured fairly well by all of the approaches, though the PQ approaches tend to underpredict the pitch response in this frequency range. Due to the resonance, small deviations of the wave loads and/or the damping can result in differences among simulations. Every modeler was free to choose his/her own approach to account for the damping and the wave excitation. As a consequence, the predictions of the responses around the resonance frequencies in surge and pitch are far less consistent between the different simulation tools than those in the wave-frequency region, as evident from the response metrics in Figure 6.

This discrepancy represents an important limitation in the propagation of systematic uncertainty through the use of simulation models. Can a simulation tool accurately propagate uncertainty in a metric that it does not accurately represent? As shown in Figure 6, there is varying levels of agreement for the low-frequency PSD sums between simulation and experiment, with the simulations sometimes over-predicting the metric value (e.g., FAST and FAST_PQ for the white noise cases), but mostly under-prediction. Since there is a reasonable level of agreement for some tools, it is assumed that the physics included in the numerical simulation tools should be able to capture the relative change in platform responses due to

small modifications in the input. The consistency of the propagated uncertainty between different modeling approaches will later be examined to assess the validity of this statement.

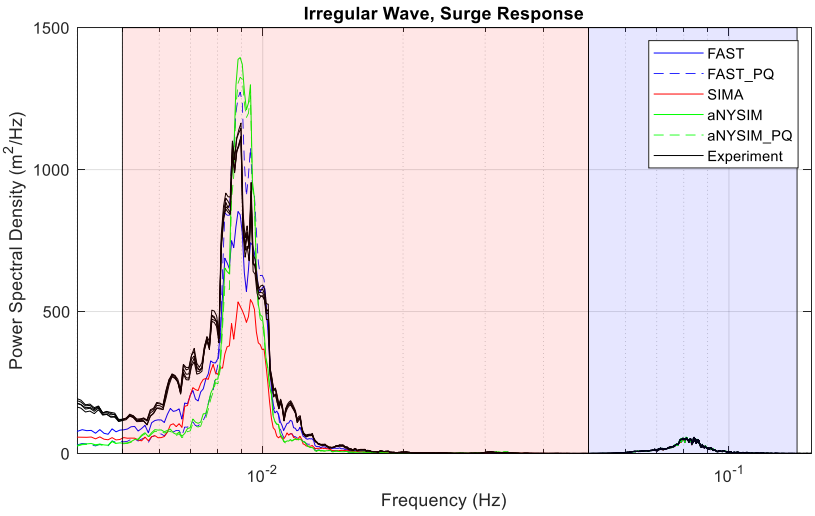

Figure 2: Power spectral density (log scale abscissa) of platform response in surge for irregular wave excitation; pink shading indicates low-frequency range for metric definition and blue indicates wave-frequency range. All experimental realizations are shown.

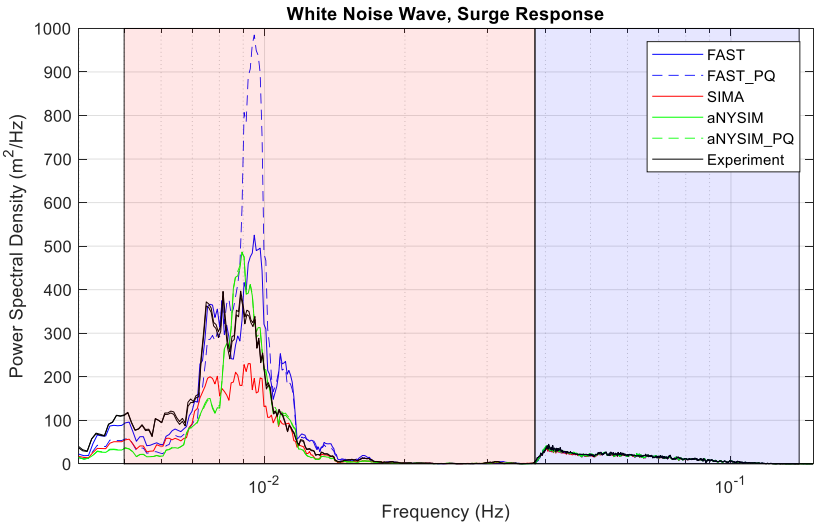

Figure 3: Power spectral density (log scale abscissa) of platform response in surge for white noise wave excitation; pink shading indicates low-frequency range for metric definition and blue indicates wave-frequency range. All experimental realizations are shown.

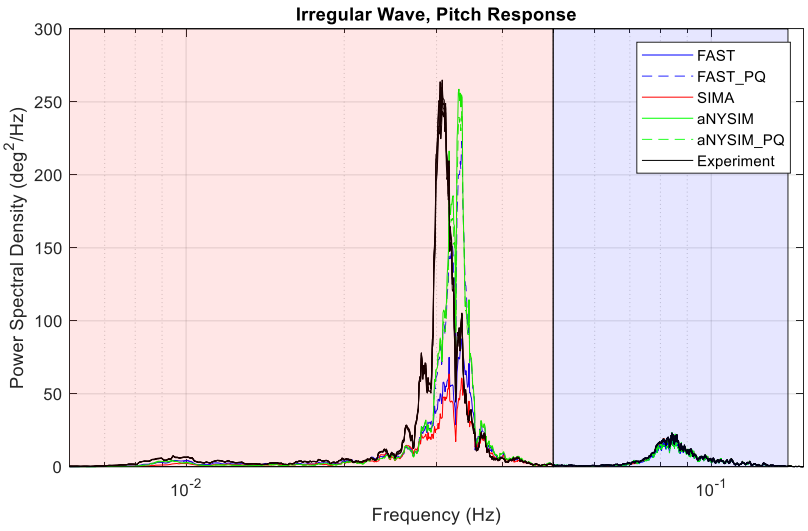

Figure 4: Power spectral density (log scale abscissa) of platform response in pitch for irregular wave excitation; pink shading indicates low-frequency range for metric definition and blue indicates wave-frequency range. All experimental realizations are shown.

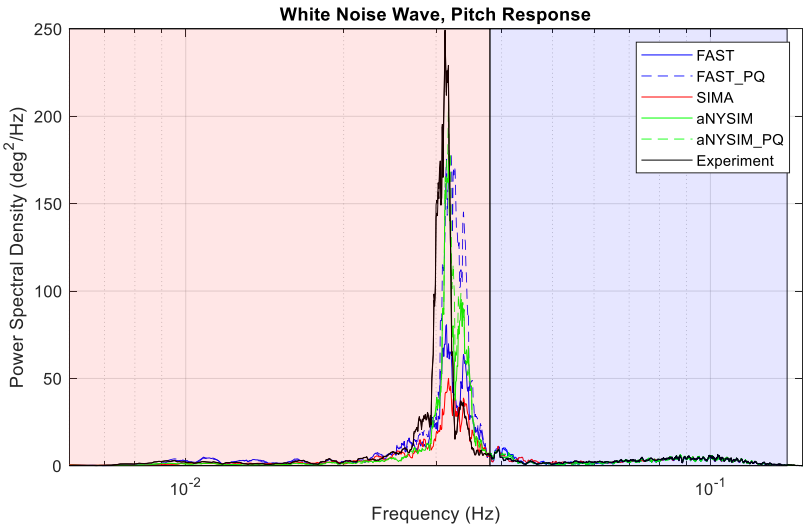

Figure 5: Power spectral density (log scale abscissa) of platform response in pitch for white noise wave excitation; pink shading indicates low-frequency range for metric definition and blue indicates wave-frequency range. All experimental realizations are shown.

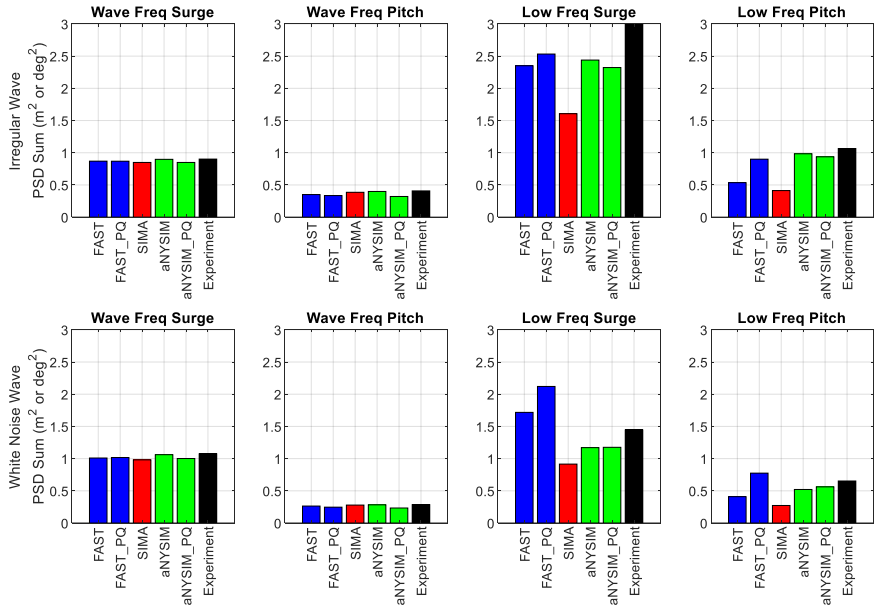

Figure 6: PSD sums: comparison of baseline simulations and measurements.

5.55.4 Implementation of Parameter Variations in Numerical Models

The parameter variations considered for the assessment of the systematic uncertainty were implemented with different approaches in the different numerical models. Differences arose because every numerical model has inherently different ways of specifying key modelling parameters. The goal was to isolate modifications to the model properties to only one parameter at a time; but, based on the modeling approach employed, this was not always possible. The different realizations of the model parameter variations for each modelling tool are outlined below.

Variation 1) CM, x direction, **Variation 2)** CM, z direction, **Variation 7)** Inertia, Iyy

The systematic uncertainty related to variations in the offset of the system center off mass in the x- and z-directions is investigated with Variation-1 and Variation-2. The x-offset value was specified as +/- 0.22 m and the z-offset was specified as +/-0.21 m respectively.

FAST and SIMA: For the CM change, only the CM is moved, there is no change in the moment of inertia. Similarly, for Variation 7, only the inertia is changed.

aNySIM: In MARIN's simulation tool, the inertia moments are defined at the center of mass. As a consequence, shifting the CM resulted in a change of moments of inertia. For instance, Variation 1 resulted in a change in the pitch period of about 2%. For variation 7, the inertia is changed independently of the mass by defining a new radius of inertia for the pitch rotation. The pitch period varied of 0.3% as a result of this inertia variation.

Variation 3) Mooring stiffness

For Variation 3, the systematic uncertainty related to variations in the mooring stiffness is investigated.

FAST and SIMA: For Variation 3, the mooring line stiffness was varied by changing EA together with the unstretched line length (+/- 2.732 m) to ensure that the mooring pre-tension did not change.

aNySIM: Variation 3 led to a small change of the pitch period of about 0.02%. The simulation tool accepts the stiffness and pre-tension directly as input parameters while the unstretched length is automatically adjusted.

Variation 4) Draft, **Variation 5)** Column diameter

The systematic uncertainty related to variations in the platform draft (+/- 0.25 m) and column diameter (+/- 0.1 m) are investigated with Variation 4 and Variation 5.

FAST and SIMA: To model the impact of changes in the platform draft and column diameter on the hydrodynamic loads without adjusting any additional model parameters (e.g. mass or line tension), the first-order potential flow solution was updated by adjusting the platform geometry mesh that is used in WAMIT. This leads to updated hydrodynamic databases for the radiation and diffraction loads. The hydrostatic restoring matrix is also updated to account for the changes in buoyancy force, center of buoyancy, and waterplane moment of inertia. The Morison-type drag forces on the columns were also updated to reflect the changes in geometry. Note that the 2^{nd}-order solution was not updated.

aNySIM: For variations 4 and 5, the corresponding change of volume was used to scale the potential flow database based on the displacement. For the draft variation, the volume was estimated to vary by 0.7%. For the column diameter variation, the volume was estimated to vary by 1.2%. Froude scaling was applied to all quantities resulting from the potential flow calculation (i.e. 1^{st} order quantities and the quadratic transfer functions). The linear hydrostatics were updated based on the new submerged geometry (displacement, center of buoyancy, waterline area second moment) while the position of the center of mass with respect to the keel was kept unchanged. When used, the diameter of the Morison elements representing the heave plates was changed with the same value as the diameter of the columns.

Variation 6) Wave Elevation

ALL: A potential 3 cm drift in the wave elevation measurement was estimated based on measurements before and after the wavemaker started. This uncertainty was addressed by adjusting the input wave elevation by a multiplicative factor. This multiplicative factor considered the 3 cm drift as the error in a representative wave amplitude. For the irregular waves with 7.1 m Hs, this factor was thus 1±0.00845.

Variation 8) Mass

FAST and SIMA: The mass of the floater was adjusted based on the assessed uncertainty. To avoid changing the draft of the structure, another parameter needed to be adjusted to achieve the

same equilibrium position. Since the displaced volume of the structure was not directly measured, it was determined to alter this value in conjunction with the mass. The displaced volume was altered by +/- 85.4 m^3 in order to maintain the same equilibrium position. The wave excitation loads were not modified due to the change in volume.

aNySIM: In the same way as for FAST and SIMA, the displacement was modified in conjunction with the mass to avoid changing the draft. Moreover, the radius of inertia was altered to keep the moment of inertia unchanged. This was done for roll, pitch and yaw.

6 Total Uncertainty

6.1 Combining all uncertainty sources

Once the total estimated systematic and random uncertainty values are calculated, they are combined to determine the total combined uncertainty, u_C for a given output metric:

$$u_C = \sqrt{(b_R)^2 + (s_{\bar{x}})^2}$$

Confidence intervals are then assigned to this uncertainty to define the expanded uncertainty (U):

$$U = ku_C$$

where k is the coverage factor. When the expected distribution of the measured data is approximately normal and the effective degrees of freedom (DOF) are large, confidence intervals of 95% to 99% are typically used, which results in a coverage factor of approximately 2 to be applied to the uncertainty bound (Kim and Hermansky, 2014). A representation of a response metric, X, is then given as:

$$X = \bar{X} \pm U$$

where X is the best available estimate of the measurement, $\bar{X}$ is the mean of the response metric, U is the expanded uncertainty, and X-U and X+U define the uncertainty bounds that would include a large portion of the possible occurrences of the response metric.

However, when there is asymmetry in the uncertainties, the definition of the expanded uncertainty bounds must be adjusted. This is accomplished by defining a displacement, q, between the center of each nonsymmetrical systematic uncertainty interval and the average:

$$q_i = \frac{(\bar{X} + b_i^+) + (\bar{X} - b_i^-)}{2} - \bar{X}$$

This displacement value is used to reinsert the asymmetry so that the total uncertainty interval is nonsymmetrical:

$$X = \left(\bar{X} + \sum_{i=1}^{N} q_i\right) \pm U$$

When there is more than one nonsymmetrical uncertainty source, the q values are summed algebraically to provide an overall asymmetry level across all nonsymmetrical sources.

In the present work, when accounting for the uncertainty contributions from different simulation tools, the largest positive and negative contributions (out of all simulation approaches) are kept for each parameter variation.

6.2 Total uncertainty values

The calculated uncertainty values for each of the four metrics are shown in Figure 7 - Figure 9. The mean metric values, shown as a square, are calculated from the response measurements averaged over all of the repeated tests. The calculated uncertainty bands are shown using error bars, and represent the expanded uncertainty (+/-U) that includes both systematic and random uncertainty sources.

Figure 7 shows significant uncertainty in the mean surge metric, especially for the regular wave cases. The mean surge value was typically small, so small changes due to parameter variations can create significant levels of uncertainty in this metric. The main source of the uncertainty in mean surge position was related to the center of mass in the x-direction (CMx) for regular wave case 1, while the mooring pretension and stiffness also contributed for the other waves. The uncertainty in mean surge in regular wave case 1 is probably overstated: the large variation was only seen for one of the simulation tools, and much of the difference is likely related to static effects (which would have been zeroed out in the experimental measurements).

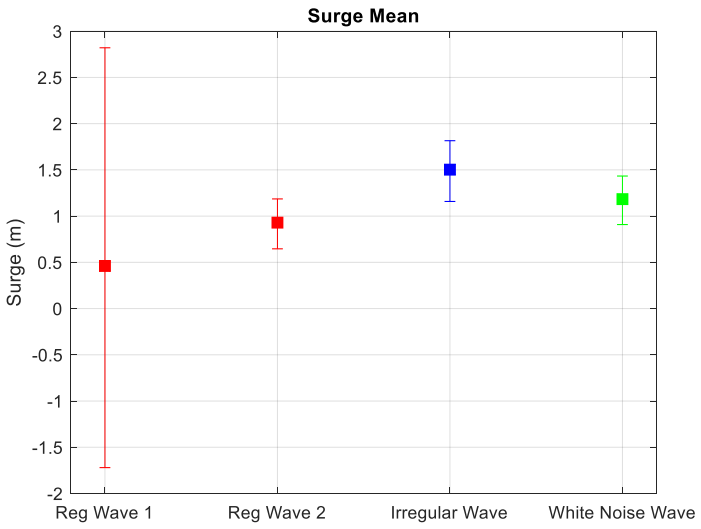

Figure 7: Mean surge metric for each wave case. The square indicates the mean value across all repeat tests, and error bars indicate the uncertainty bounds

Figure 8 shows the experimentally obtained RAOs for the irregular and white noise waves – averaged over the repetitions and smoothed. Plotted on top of these curves are the six frequency points computed for each of the waves, including the expanded uncertainty. Where multiple repetitions are available, the mean of all of the repetitions is shown. There is generally good agreement in the experimentally obtained RAOs between different wave conditions. Although some larger discrepancies can be observed in the pitch RAO at a given frequency, individual wave RAO values fit within the error bars for other wave RAO values. The uncertainty level depends on the frequency. The uncertainty in the low-frequency responses is larger than the uncertainty at higher frequencies. The trend toward higher uncertainty at low frequencies is observed in most of the uncertainty parameters, suggesting that the main reason may be related to the increasing importance of 1) damping since the excitation frequency approaches the natural frequency (especially in heave and pitch) and 2) cancellation effects in the excitation (which depend strongly on the geometry). Although the uncertainty level at a given frequency is similar for all considered waves, it is not identically reproduced. The main conclusions from Figure 8 are that the uncertainty in the wave-frequency responses is generally small for wave periods shorter than approximately 14 seconds, and that the pitch responses are more uncertain than surge responses.

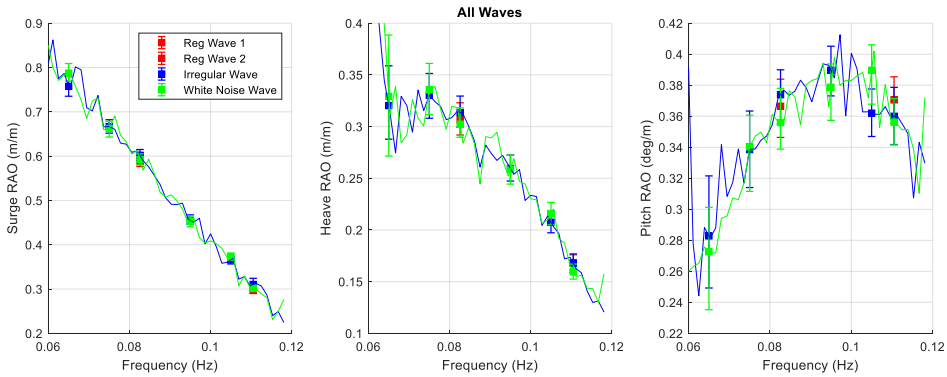

Figure 8: Comparison of RAO values across wave cases. Mean results at the selected frequencies (for each wave) are shown by squares, and error bars indicate the uncertainty bounds for those frequencies. Lines show the experimentally obtained RAOs by irregular and white noise waves.

The focus of this test campaign is on the low-frequency response of the wind turbine in the surge and pitch DOFs. Figure 9 shows the PSD sum metric for both the irregular and white noise wave in these two DOFs in both the wave and low-frequency regions. The uncertainty levels vary between the two irregular waves (irregular and white noise); the difference is especially pronounced in the low-frequency surge metric. The amplitude of the total uncertainty in the wave-frequency PSD sum metric is less than 20%, while the low-frequency PSD sum metric for surge is on the order of 30-50% and the low-frequency PSD sum metric for pitch is approximately 40% for the white noise wave case.

6.3 Contributions to uncertainty

To understand what is driving these uncertainties, the individual uncertainty sources (b_i and $s_{\bar{x}}$) are shown in Figure 10. This figure indicates that the high uncertainty levels in the surge direction come from uncertainty in the mooring stiffness for the low-frequency response and from the wave elevation, column diameter and mass/buoyancy for the wave-frequency response. In the pitch direction, uncertainty in the center of mass offset, and also column diameter and draft, create the largest levels of uncertainty in the response. These results highlight the fact that the low-frequency responses, which are primarily resonant responses, are especially sensitive to parameters that affect the stiffness of the system and the inertia of the system. Changes in stiffness or changes in inertia may shift the natural frequency slightly, and the level of excitation at the resulting natural frequency may differ compared to the original system. Figure 10 also confirms that the contribution of the random uncertainty to the total uncertainty is negligible compared to the systematic uncertainty.

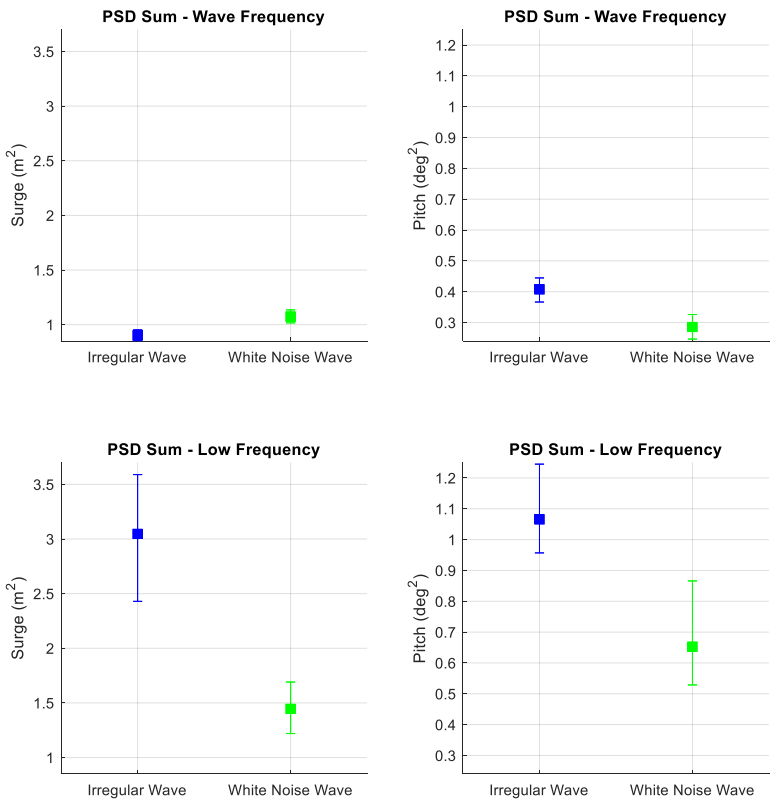

Figure 9: PSD sum metrics for the irregular and white noise wave cases, in both pitch and surge directions; square indicates the mean value across all repeat tests, and bars indicate the uncertainty bounds

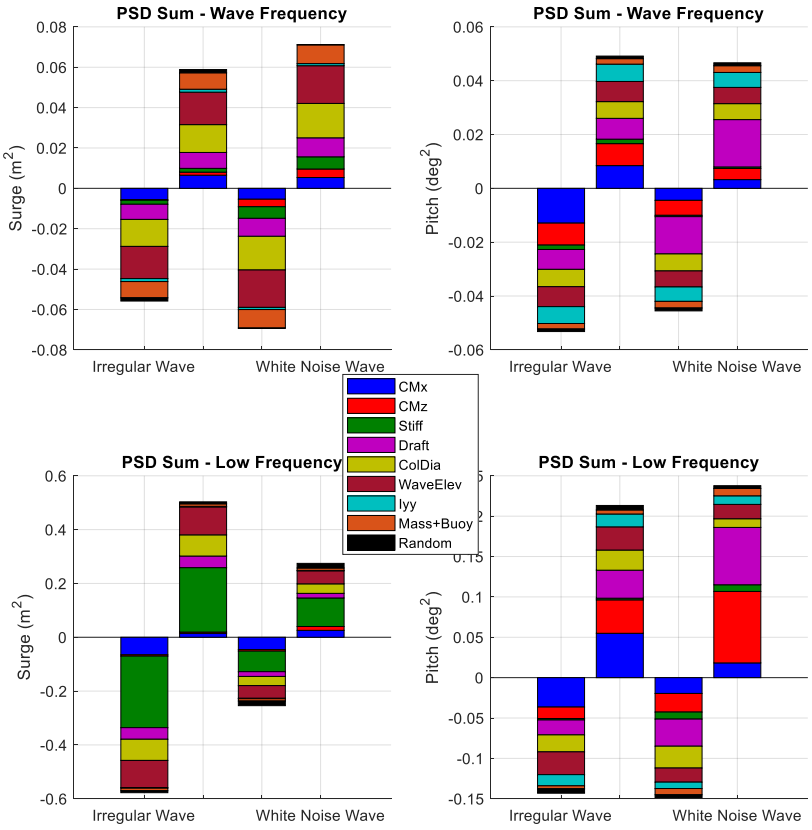

Figure 10: Break-down of sources of uncertainty (random and individual systematic sources) for the PSD sum metric

Figure 11 and Figure 12 examine the variability in the level of propagated uncertainty for these uncertainty sources based on what modeling tool is used, considering two of the low-frequency response metrics with large uncertainty: surge in the irregular wave in Figure 11 and pitch in the white noise wave in Figure 12. The contributions from each tool for each parameter variation, both positive and negative, are included. The different simulation tools generally agree regarding *which* parameters give the largest contributions to uncertainty, such as the mooring stiffness and pretension for the low-frequency surge, and mostly agree on the direction of the largest changes (i.e. positive or negative change in the metric). On the other hand, there are significant variations in the magnitude of the changes in the metric depending on which simulation tool is applied.

It is important to note that the changes in metrics from different parameter variations are additive, and that only the largest variations (among different simulation tools) are used in the calculation of total uncertainty. As a result, the total uncertainty in this study is more conservative than if one had only used a single simulation tool. There is not a clear pattern suggesting that the PQ- or Morison-type approaches give larger uncertainty for particular parameter variations, but a closer correlation can be noted based on simulations using the same modelling tools (comparing, for example, surge results with aNySIM_PQ and aNySIM, or results from FAST and FAST_PQ). Nonetheless, it is impossible to determine whether or not the use of engineering models to predict low-frequency responses will give a conservative or non-conservative estimate of the total uncertainty.

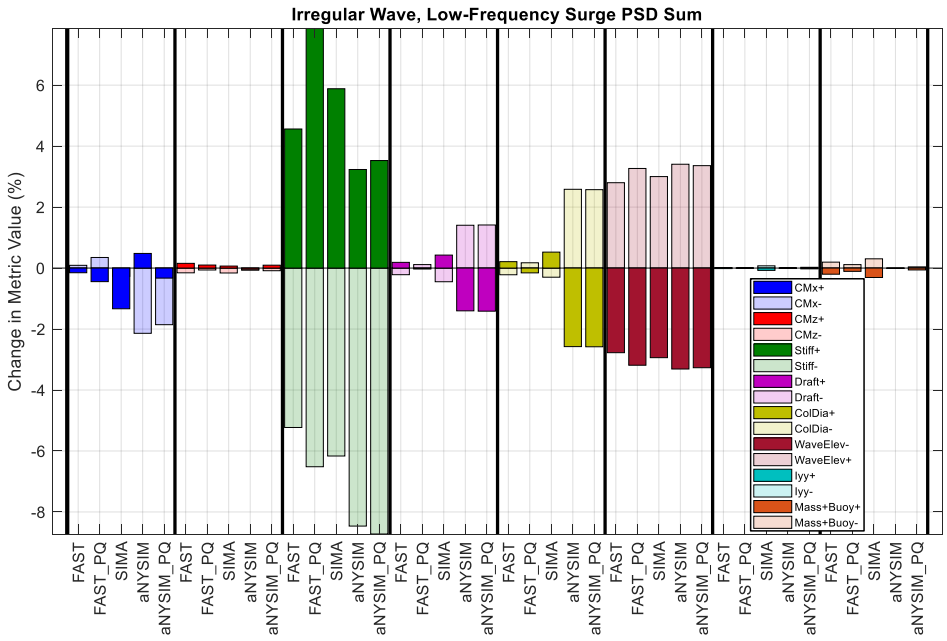

Figure 11: Variability of propagated uncertainty for the irregular, low-frequency surge PSD sum metric, based on a variety of modelling approaches; positive metric variations are in bold and negative are shown in a muted color

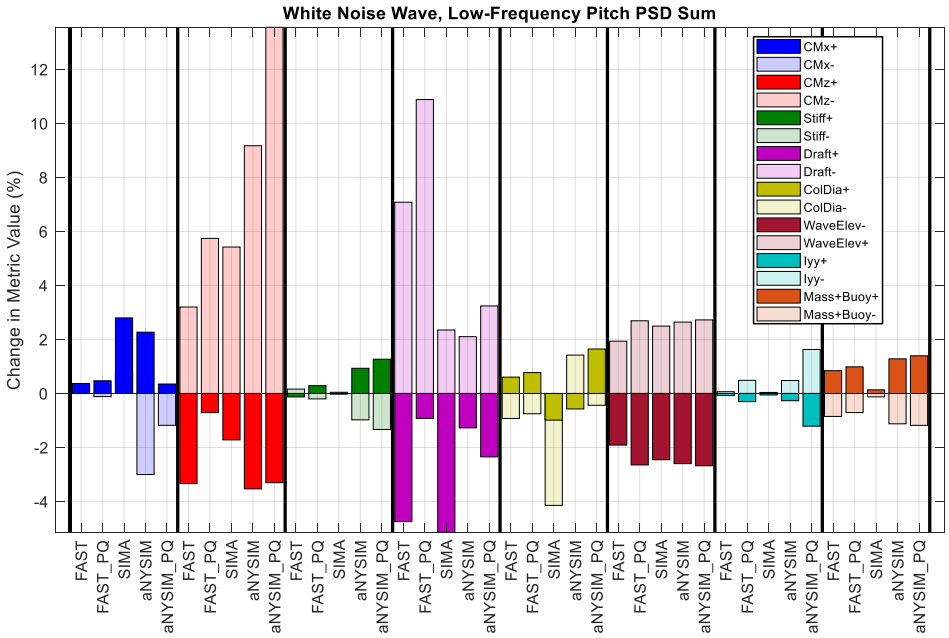

Figure 12: Variability of propagated uncertainty for the white noise, low-frequency pitch PSD sum metric, based on a variety of modelling approaches; positive metric variations are in bold and negative are shown in a muted color

6.4 Application to OC5 results

In order to understand the magnitude of the experimental uncertainty with respect to numerical simulations, the original OC5 study results (Robertson et al. 2017) are re-visited here. The experimental tests which were studied in the OC5 project correspond to a different physical model, in a different basin, but under similar wave conditions (LC3.3 from Robertson et al. 2017). As shown in Figure 13 and Figure 14, the PSD sums were computed for both the experimental and numerical results in the OC5 study, and the relative uncertainty from the present tests was applied to the original experimental results. For the low-frequency surge metric, only one of the numerical results (out of 21 participant results) was within the error bounds on the experimental result – even after several iterations and tuning. None of the simulation tools predicted the low-frequency pitch response within the experimental uncertainty. It should be noted that the tuned PQ approach used for the uncertainty propagation in this paper, which shows promise in estimating these low-frequency metrics, is not represented in the OC5 study. This modeling approach, as well as others, were developed as a direct consequence of the issues identified in OC5.

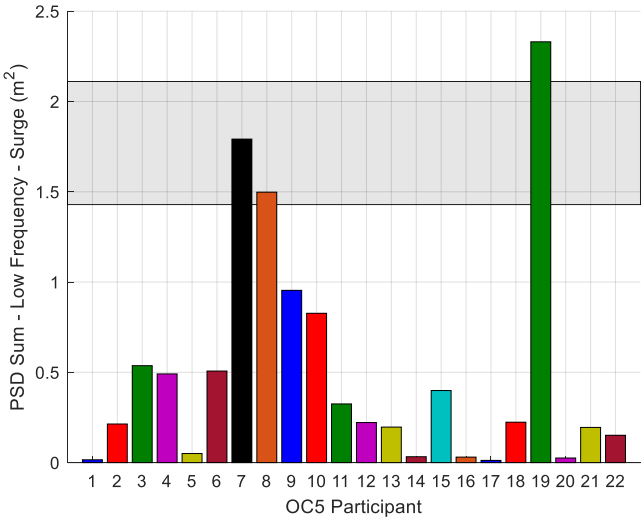

Figure 13: Low-frequency surge PSD sum metric for the original OC5 results (Robertson et al. 2017), with experimental uncertainty indicated based on the present work. OC5 participant 7 (black) refers to the experimental results.

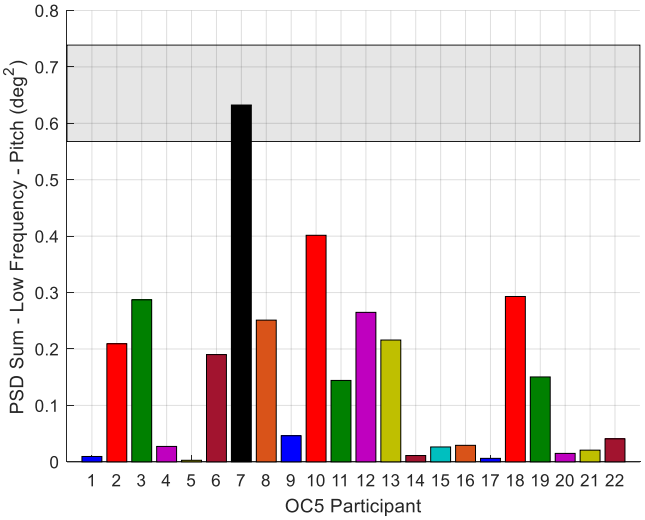

Figure 14: Low-frequency pitch PSD sum metric for the original OC5 results (Robertson et al. 2017), with experimental uncertainty indicated based on the present work. OC5 participant 7 (black) refers to the experimental results.

7 Conclusions

The total experimental uncertainty in a set of hydrodynamics model tests with a rigid semisubmersible wind turbine has been estimated through propagation of the systematic uncertainties using several numerical simulation tools. Considering response metrics which give an indication of the wave-frequency and low-frequency responses of the system, the wave frequency responses are found to have relatively small uncertainty, while the uncertainty in the low-frequency responses is somewhat higher (20-40% in the integral of power spectral density over a defined low-frequency range). The random uncertainty, which was found through repeated measurements, is negligible compared to the estimated systematic uncertainty.

The main contributions to the propagated systematic uncertainty in low-frequency responses were primarily model characteristics that affected the stiffness: mooring system stiffness for the surge response, and platform draft, and vertical center of gravity for the pitch response. In addition, uncertainty in the wave amplitude also had an impact. The simulation tools applied in the study showed good agreement regarding which parameters were most important, although the magnitude of the propagated uncertainty differed significantly among participants.

A major limitation in the present work is the use of simulation tools for uncertainty propagation: the inconsistent estimation of the baseline value of the low-frequency PSD sums suggests that the modelling tools may not be sufficiently accurate to be used for uncertainty propagation. At present, however, these tools represent the state-of-the-art, and the results of the present study suggest that the differences between experiments and simulations are larger than the uncertainty in the experimental results.

The results from this study give a measurement of uncertainty that can be used in future validation efforts: the data from the present tests will be studied further using both engineering and high-fidelity models through the OC6 extension of the Offshore Code Comparison Collaboration through the International Energy Agency. Additional tests, where wave and radiation loads were measured directly on the fixed structure, will also be incorporated in the OC6 project in order to better understand the reasons for discrepancies between simulations and experiments.

Acknowledgments

The authors would like to acknowledge the support of the MARINET2 project (European Union's Horizon 2020 grant agreement 731084), which supplied the tank test time and some travel support to accomplish the experimental testing campaign. The support of MARIN in the preparation, execution of the model-tests, and the evaluation of the level of different sources of uncertainties was essential for this study. MARIN's contribution was partly funded by the Dutch Ministry of Economic Affairs through TKI-ARD funding programs.

This work was partially supported by the U.S. Department of Energy under Contract No. DE-AC36-08GO28308 with the National Renewable Energy Laboratory. Funding for the work was provided by the DOE Office of Energy Efficiency and Renewable Energy, Wind Energy Technologies Office.

References

1. ASME (2013). "Test Uncertainty, Performance Test Codes," ASME PTC 19.1-2013.
2. Berthelsen, P. A.; Bachynski, E. E.; Karimirad, M. and Thys, M. (2016) Real-time Hybrid Model testing of a Braceless Semisubmersible Wind Turbine. Part III: Calibration of a Numerical Model. in Proceedings of the ASME 2016 35th International Conference on Ocean, Offshore and Arctic Engineering OMAE2016, Busan, Korea, June.
3. Buchner et al. (2001). "Numerical Multiple-Body Simulations of Side-by-Side Mooring to an FPSO", Proc. of IOPEC 2001.
4. Cermelli CA, Roddier DG. Experimental and Numerical Investigation of the Stabilizing Effects of a Water-Entrapment Plate on a Deepwater Minimal Floating Platform. ASME. International Conference on Offshore Mechanics and Arctic Engineering, *24th International Conference on Offshore Mechanics and Arctic Engineering: Volume 2* ():517-525. doi:10.1115/OMAE2005-67077.

3. Clifton, A.; Daniels, M. Lehning, M. (2014). "Effect of winds in a mountain pass on turbine performance". Wind Energy 17 (10) (2014) 1543e1562.

4.6. Figliola, R. and Beasley, D. (2011) "Theory and Design for Mechanical Measurements (Fifth Edition)," John Wiley and Sons, Inc.

5.7. Goupee, A. J., Fowler, M. J., Kimball, R. W., Helder, J. and de Ridder, E.-J. (2014) Additional wind/wave basin testing of the DeepCwind semisubmersible with a performance-matched wind turbine. in Proceedings of the ASME 2014 33rd International Conference on Ocean, Offshore and Arctic Engineering OMAE2014, San Francisco, California, USA, June.

6.8. Goupee, A. J., Koo, B. J., Lambrakos, K. F. and Kimball, R. W. (2012) Model Tests for Three Floating Wind Turbine Concepts. in Offshore Technology Conference.

7.9. Gueydon, S. (2017) MARINET2 OC6 Model-tests MARIN. *To be published on MARIN's website.*

8.10. Gueydon, S., Duarte, T., Jonkman, J. Comparison of Second-Order Loads on a Semisubmersible Floating Wind Turbine. in Proceedings of the ASME 2014 33rd International Conference on Ocean Offshore Mechanics and Arctic Engineering OMAE2014, San Francisco, United States, June.

9.11. Gueydon, S., 2016. "Aerodynamic Damping on a Semisubmersible Floating Foundation for Wind Turbines," Energy Procedia (2016) pp. 367-378, DOI: 10.1016.

10.12. ISO (1993). "Guide to the Expression of Uncertainty in Measurement," International Standards Organization, Geneva, Switzerland.

11.13. ITTC (2008). "Guide to the Expression of Uncertainty in Experimental Hydrodynamics," Recommended Procedures and Guidelines, 7.5-01-01.

12.14. Jonkman, J. (2010) Definition of the Floating System for Phase IV of OC3.

13.15. Jonkman, J., Butterfield, S., Musial, W. and Scott, G. (2009) Definition of a 5-MW Reference Wind Turbine for Offshore System Development National Renewable Energy Laboratory.

14.16. Kim, Y. and Hermansky, G. (2014). "Uncertainties in seakeeping analysis and related loads and response procedures," *Ocean Engineering*, 86, 68-81.

17. Masciola, M, Jonkman, J, and Robertson, A (2013). "Implementation of a Multisegmented, Quasi-Static Cable Model," Proc Twenty-Third International Offshore and Polar Engineering, Anchorage, AK.

18. Manteufel, R. (2012). "Sequential Perturbation Uncertainty Propagation in Thermal-Fluid Applications." Proceedings of the ASME 2012 International Mechanical Engineering Congress & Exposition, Nov. 9-15, 2012, Houston, TX.

15.19. Murcia, J.P.; Rethor, P. Dimitrov, N.; Natarajan, A.; Sørensen, J.; Graf, P.; Kim, T. (2016). "Uncertainty propagation through an aeroelastic wind turbine model using polynomial surrogates." Renewable Energy 2017, https://doi.org/10.1016/j.renene.2017.07.070.

16.20. Philippe M, Courbois A, Babarit A, Bonnefoy F, Rousset J, Ferrant P. Comparison of Simulation and Tank Test Results of a Semisubmersible Floating Wind Turbine Under Wind and Wave Loads. ASME. International Conference on Offshore Mechanics and Arctic Engineering, *Volume 8: Ocean Renewable Energy*:V008T09A081. doi:10.1115/OMAE2013-11271.

17.21. Robertson, A. N., Wendt, F., Jonkman, J. M., Popko, W., Dagher, H., Gueydon, S., Qvist, J., Vittori, F., Azcona, J., Uzunoglu, E., Soares, C. G., Harries, R., Yde, A., Galinos, C., Hermans, K., Vaal, J. B. d., Bozonnet, P., Bouy, L., Bayati, I., Bergua, R., Galvan, J., Mendikoa, I., Sanchez, C. B., Shin, H., Oh, S., Molins, C. and Debruyne, Y. (2017). "OC5 Project Phase II: Validation of Global Loads of the DeepCwind Floating Semisubmersible Wind Turbine". *Energy Procedia*, Vol 137, pp. 38-57.

22. Robertson, A. N., Bachynski, E.E., Gueydon, S. Wendt, F., Schünemann, P., and Jonkman, J. (2018). "Assessment of experimental uncertainty for a floating wind semisubmersible under hydrodynamic loading." *Proceedings of the ASME 2018 37th International Conference on Ocean Offshore Mechanics and Arctic Engineering*, Madrid, Spain.

23. WAMIT, Inc. (2011). *WAMIT User Manual Version 6.1, 6.1PC, 6.1S, 6.1S-PC.* Chestnut Hill, MA.